

Supplementary Information

S1. ECHAMP Inlet Description

A schematic of the ECHAMP inlet used during SAFS is shown in Fig. S1. As described in the main text, the inlet was mounted approximately 15 m above ground level. Solenoid valves were located inside the AML, and gases were transported to the inlet through 22.8 m of 3.2 mm (1/8") OD FEP tubing for NO and copper tubing for N₂ and C₂H₆. At any given point in time, one reaction chamber was in amplification mode (C₂H₆ added upstream, N₂ added downstream) and the other was in background mode (N₂ added upstream, and C₂H₆ added downstream). This inlet differs from that described in Wood et al. (2017) in that a RO_x calibration system based on water vapor photolysis (described in Sect. S2.1) was permanently connected to the inlet, so that calibrations could be performed without disturbing sampling from the other instruments. During calibrations, zero air was delivered by 22.8 m of 9.5 mm (3/8") OD FEP tubing to a 12.7 mm (0.5") OD quartz tube inside the inlet box

S2. XO₂ Calibrations

Total peroxy radicals were calibrated using two methods: photolysis of H₂O followed by reaction with either H₂ or C₂H₆ and photolysis of CH₃I. We described both methods here.

S2.1. H₂O calibration

Calibration of XO₂ was performed via water vapor photolysis at 184.9 nm from a mercury lamp, which produces an equimolar mixture of OH and HO₂, according to Reaction (RS1) (Schultz et al., 1995; Lanzendorf et al., 1997). The OH was then reacted with H₂ (g) which was added to the zero air flow upstream of the UV illumination to quantitatively convert OH into HO₂ (Reaction RS2).



Total XO₂ can then be calculated from Eq. (S1), where brackets denote concentration, σ and ϕ are the absorption cross sections and photolysis quantum yields at 185 nm for the indicated species, respectively. For $\sigma_{\text{H}_2\text{O}}$ we use $7.1 \times 10^{-20} \text{ cm}^2 \text{ molecule}^{-1}$ (Cantrell et al., 1997). The effective O₂ absorption cross section depends on both the UV lamp operating conditions and the O₂ column density

27 and therefore and must be characterized for each lamp (Lanzendorf et al., 1997;Creasey et al., 2000). The
28 Hg lamp used in this study was characterized at the University of Indiana courtesy of Phil Stevens and
29 found to have an effective cross section of $1.3 \times 10^{-20} \text{ cm}^2 \text{ molecule}^{-1}$ at an O_2 column density of 5×10^{18}
30 molecules cm^{-3} , within the range of values seen in other studies (Lanzendorf et al., 1997;Creasey et al.,
31 2000). Quantification of the ozone formed by photolysis of O_2 at the same wavelength (184.9 nm) serves
32 as the “chemical actinometer” (Schultz et al., 1995).

$$[HO_2] + [RO_2] = \frac{[O_3][H_2O]\sigma_{H_2O}\phi_{H_2O}}{[O_2]\sigma_{O_2}\phi_{O_2}} \quad (\text{S1})$$

33

34 The typical calibration procedure is as follows:

- 35 1. 8 to 10 LPM of dry zero air (ZA) flow sequentially through 22.8 m of 9.5 mm (3/8”) OD FEP
36 tubing, an 18 cm long 12.7 mm (0.5”) quartz tube in the ECHAMP inlet box, and into the
37 sampling manifold (see Fig. S1). Both reaction chambers are operated in background mode, with
38 NO and N_2 added upstream of the reaction chambers and ethane added downstream. The NO_2
39 concentration measured by the CAPS sensors for this step is solely from impurities in the NO
40 flow and NO_2 formed by the termolecular reaction between NO and O_2 .
- 41 2. A mercury lamp (Jelight 78-2046-2) mounted onto the outside of the quartz tube is then turned
42 on, providing UV radiation at 184.9 nm and resulting in the production of O_3 in the ZA flow but
43 no HO_x given the absence of $\text{H}_2\text{O}_{(\text{g})}$. A nitrogen purge was placed between the lamp and the
44 quartz tubing to prevent ozone formation outside of the sampling system. Only a small portion of
45 the quartz tubing (~1 cm) is exposed to the lamp to control the eventual HO_x and O_3
46 concentrations. The ozone reacts with the excess NO to produce NO_2 . The ozone concentration
47 for Eq. (S1) is thus given by the difference in measured $[\text{NO}_2]$ between steps 1 and 2 of the
48 calibration, with a 10% correction applied to account for the dilution by the added flows of NO,
49 N_2 , and C_2H_6 . Typical O_3 concentrations for calibration were between 0.5 and 2 ppbv, which is

50 easily measured with the CAPS sensors given their typical NO₂ precision of 20 pptv with 10-
51 second averaging.

52 3. A portion of the ZA is then sent through a bubbler system with distilled water to humidify the ZA
53 flow. The H₂O concentration for Eq. (S1) is calculated using the RH and temperature reading
54 from the Vaisala probe and the ambient pressure.

55 4. H₂ gas was then added to the mixture at a flow rate of 30 sccm. ECHAMP was then operated in
56 normal sampling mode, with the two reaction chambers alternating between amplification and
57 background modes every 60 s.

58 The amplification factor, F, is then determined from the ratio of the observed change in NO₂ signal
59 during step 4 (amplification mode) to the XO₂ concentration calculated from Eq. (S1).

60 61 ***S2.2. CH₃I calibration***

62 The CH₃I photolysis method, similar to the acetone photolysis method described in Wood and
63 Charest (2014) except that methyl iodide is used in place of acetone, produces methyl peroxy radicals
64 (CH₃O₂) by the UV photolysis of CH₃I(g):

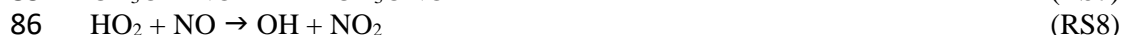


68
69 In both cases, the peroxy radical concentration is quantified simply by the increase in NO₂ following
70 reaction of the peroxy radicals with excess NO. The concentration quantification does not rely on
71 spectroscopic parameters or direct actinometry of the UV source, but instead on the accuracy of the NO₂
72 measurements by the CAPS, which we trace to the absorption cross section of O₃ at 254 nm, and the
73 relative rate constants for reactions.

74 The source of CH₃I is a permeation tube (KynTek, 1.8 μg/min permeation rate at 35° C), held at
75 55° C. We flow approximately 100 sccm of N₂ through the permeation tube and dilute this into a larger
76 flow of 8 LPM of either dry or humidified ultra zero air, resulting in an estimated CH₃I mixing ratio of 80
77 ppbv based on the manufacturer-stated permeation rate and assuming the permeation rate is twice as high

78 at 55° C. This diluted CH₃I then enters a Pyrex photolysis chamber (volume 50 cm³) into which an “O₃-
79 free” mercury lamp is inserted (Jelight model 81-3306-2, all 185 nm radiation blocked).

80 When these CH₃O₂ radicals enter the reaction chamber that is in “background” mode, i.e., with
81 the C₂H₆ added downstream of the NO addition, allowing time for all sampled RO_x to be converted to
82 HONO, the following reactions occur:



87

88 Thus by modulating the CH₃O₂ source and observing the change in NO₂, the concentration of CH₃O₂ can
89 be calculated based on the overall stoichiometry of Reactions (RS5) through (RS8). Modulating the NO
90 flow on and off instead of the CH₃O₂ source would be inferior because it would also remove the NO₂
91 already present in the NO flow due to impurities and the termolecular reaction between NO and O₂. The
92 CH₃O₂ flow can be modulated in three ways: 1. Periodically diverting the CH₃I flow from the perm tube
93 away from the air dilution flow (but with the zero air still illuminated by the UV lamp), 2. Turning the
94 UV source on and off, or 3. Periodically having the diluted CH₃I + zero air flow bypass the UV chamber
95 and proceed to the ECHAMP inlet.

96 Method 1 is similar to the acetone photolysis method described by Wood and Charest (2014) with the
97 weakness that it will also remove any interfering species present in the permeation tube output that absorb
98 blue light, e.g., I₂ or I₃⁻ compounds. The advantage of methods 2 and 3 are that any blue-absorbing species
99 present in the gas mixture will always be present and thus not present an interference. This is important
100 when using the CAPS monitor to quantify NO₂, since it measures the total cell absorption at 450 nm
101 (FWHM 10 nm) and thus is not completely spectroscopically selective to NO₂. Method 2 suffers from the
102 time required for the Hg lamp to warm-up. Method 3 is thus our primary method, though we periodically
103 use methods 1 and 2 as a check. A schematic of the calibration setup is shown in Fig. S4.

104 There are two main parts to the calibration procedure:

105 1. CH₃I flows through the UV chamber, producing CH₃O₂ radicals, and the two channels
106 of ECHAMP are operated in its standard operation mode, each channel alternating
107 between amplification mode and background mode.

108 2. Both channels are kept in background mode, and the CH₃O₂ source is modulated as
109 described above by periodically having the diluted CH₃I flow bypass the photolysis
110 chamber.

111
112 The amplification factor is given by Eq. (S2):

$$113 \quad F = \Delta\text{NO}_2(\text{step1}) / [\text{CH}_3\text{O}_2] \quad (\text{S2})$$

114
115
116 $\Delta\text{NO}_2(\text{step1})$ is the difference in [NO₂] observed by ECHAMP during step 1 of the calibration procedure
117 and [CH₃O₂] is determined by the following equation:

$$118 \quad [\text{CH}_3\text{O}_2] = \Delta\text{NO}_2(\text{step2}) / (1.86 \times 0.92) \quad (\text{S3})$$

119
120 $\Delta\text{NO}_2(\text{step2})$ is the change in [NO₂] observed when the CH₃O₂ source is modulated during step 2. The
121 factor of 1.86 accounts for the portion of the CH₃O₂ radicals that form CH₃ONO upon reaction with
122 excess NO rather than two NO₂ molecules. This is calculated by Eq. (S4):

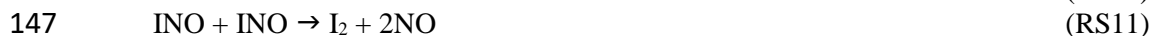
$$123 \quad FF = 2 \left\{ \frac{k_{\text{RS6}}[\text{O}_2]}{k_{\text{RS6}}[\text{O}_2] + k_{\text{RS7}}[\text{NO}]} \right\} \quad (\text{S4})$$

124
125
126 Where k_{RS6} ($1.9 \times 10^{-15} \text{ cm}^3 \text{ molecule}^{-1} \text{ s}^{-1}$) and k_{RS7} ($3.3 \times 10^{-11} \text{ cm}^3 \text{ molecule}^{-1} \text{ s}^{-1}$) are the rate constants
127 for Reactions (RS6) and (RS7), respectively (Atkinson et al., 2006). The factor of 0.92 in Eq. (S2)
128 accounts for the dilution of the gas by the added N₂, C₂H₆/N₂, and NO/N₂.

129 In contrast to the H₂O photolysis method, this CH₃I method is an “internal” calibration, i.e. the
130 concentration determined is the amount that entered the reaction chamber - it does not account for losses
131 of radicals in the sampling system. Separate wall loss measurements have demonstrated that losses of
132 CH₃O₂ in our sampling inlet are negligible (less than 1%) and losses of HO₂ less than 3%. Sampling
133 losses of CH₃O₂ and other peroxy radicals, especially HO₂, will be described in more detail in a future
134 publication (Anderson et al, in preparation).

135 An example time series of CH₃I calibration data is shown in Fig. S5 from 31 May 2017. From 10:30
136 to 10:34 ECHAMP was operating in regular sampling mode (alternating amplification-background
137 mode), sampling CH₃O₂ radicals from the CH₃I photolysis system at 23% RH, with a modulated NO₂
138 signal of 4.14 ppbv. From 10:34 to 10:40, the diluted CH₃I periodically bypassed the UV chamber,
139 producing a modulated NO₂ signal of 0.37 ppbv. This results in an amplification factor of 19.1. During
140 field calibrations we typically measure multiple single-point calibrations over a range of RH values. To
141 confirm instrument linearity we occasionally execute multi-point calibrations over a range of
142 concentrations at a single RH value.

143 We have also investigated potential interferences due to I₂ formation. I₂ can also be formed following
144 photolysis of CH₃I through the following mechanisms as described by Clemitshaw et al (1997):



150
151 The maximum amount of I₂ that could be formed, based on Reactions (RS9), (RS11), and (RS13), is
152 equal to [CH₃O₂]/2. At this amount, I₂ would be an interference as it absorbs blue light and would be
153 detected as NO₂ by the CAPS sensor (I₂ absorption cross section at 450 nm is ~75% that of NO₂).

154 To determine experimentally whether there is any observable interference from I₂ formation, we
155 determined the CH₃O₂ concentration as described in step 2 of the calibration procedure above. Then, we
156 turned off the NO flow, effectively stopping amplification. Leaving the lamp on, we then periodically
157 switched between flowing the CH₃I through the photolysis chamber and then bypassing photolysis. The
158 difference in observed signal between these two settings would therefore stem from absorption of blue
159 light from I₂. For a flow rate that produced 100 pptv of CH₃O₂, concentrations typically used for
160 calibrating, the I₂ signal, if any, was indistinguishable from the instrument noise, suggesting that at this
161 concentration, there is negligible interference from I₂ in our calibration. For a flow rate that produced a
162 CH₃O₂ concentration of 450 pptv, significantly larger than what is used for calibrations, the CAPS

163 produced an “equivalent” NO₂ signal of ~100 pptv, which would lead to an overestimate in the CH₃O₂
164 concentration of 22%.

165 A simple computer numerical integration, using the above described reactions, was also used to
166 calculate the variation in INO, I₂, and CH₃O₂I with time. Literature values were used for all rate constants
167 except for reactions S12 and S13, for which literature values could not be found. Four simulations were
168 conducted. In the first two, the rate constant for Reaction (RS12) (forward) was estimated as 1×10^{-11}
169 cm³ molecules⁻¹ s⁻¹, and the rate constant for the reverse (RS12) reaction, k was assumed to be 0. The
170 initial concentrations of I and CH₃O₂ were 100 pptv in the first simulation and 1000 pptv in the second.
171 In the third and fourth simulations, these initial concentrations were kept the same, while the reaction
172 rates for S12 was increased to 1×10^{-10} cm³ molecules⁻¹ s⁻¹. The simulations are summarized in Table S1.
173 Table S2 shows the reaction rate constants for each reaction used in the simulation.

174 Each simulation showed that I₂ formation was negligible for the conditions used in calibration. In
175 the presence of 1 ppm NO, the simulations indicated that more than 99.9% of the I is rapidly converted to
176 INO, leaving the INO self-reaction (Reaction RS14) as the only viable route to I₂ formation. The rate
177 constant for this reaction is 1.3×10^{-14} cm³ molecules⁻¹ s⁻¹ (Atkinson et al., 2007) – 30 times slower than
178 the effective 2nd-order rate constant for the direct recombination of atomic I (Reaction RS9). In addition,
179 the simulation was repeated including the reaction of I with INO to form I₂ and NO, with no significant
180 change to the results. We conclude that I₂ formation is negligible under the conditions of our calibrations,
181 in agreement with our laboratory tests.

182 ***S2.3. CH₃I calibration***

183 Figure S6 compares the CH₃I (blue circles) and H₂O photolysis (red, filled triangles) calibration
184 methods from the AQRP campaign. Both methods agree within uncertainty. Variability in the F values
185 likely results from variations in mercury lamp intensity, which during the campaign was only measured
186 when the ozone mixing ratio was quantified (via the change in [NO₂]) when the lamp was turned off. We
187 use the CH₃I derived curve in this analysis because H₂O photolysis calibrations were all conducted at RH

188 less than ~20%. Because increasing the RH also increases the HO₂ concentration in the H₂O photolysis
189 calibration method, the UV lamp output must be attenuated to prevent super-ambient radical
190 concentrations. During AQRP, a remote method of light attenuation was unavailable, and because the
191 instrument inlet box was inaccessible without interrupting sampling for other instruments, we could not
192 alter the H₂O photolysis setup. For RH greater than 20%, it was found that the resultant HO₂
193 concentration was unreasonably high (sometimes exceeding 1 ppbv), and we therefore limit results to
194 below this value. To demonstrate that the H₂O photolysis calibration method is applicable over a wider
195 range of RH, we show results from a subsequent field deployment in Bloomington, IN during July 2017
196 (Fig. S6, red, open triangles). While we would expect differences in the calibration results because the
197 instrument configuration was different for this later deployment, the overall relationship between F and
198 RH is similar at higher RH values.

199 *S3. Isoprene*

200
201 No isoprene standard was available during SAFS for online calibration of the GC-MS
202 observations. Approximately 6-months after the campaign, a calibration of the same instrument was
203 conducted during a second campaign using a multi-component mixture, including isoprene and 6 other
204 hydrocarbons measured during SAFS. To determine a sensitivity for isoprene for SAFS, the sensitivities
205 for the six hydrocarbons during SAFS was compared to that for the second campaign, in which the GC
206 setup differed in both sample trap temperature and detector micro channel plate voltage from the SAFS
207 configuration. The mean ratio of sensitivities from SAFS to the second campaign for the six overlapping
208 hydrocarbons was 0.34 ± 0.10 (1σ), while the slope of a regression line of the SAFS sensitivities to the
209 second campaign sensitivities was 0.38. The isoprene sensitivity for SAFS was then determined by
210 dividing the sensitivity at the second campaign by the average of these two values (0.36). The total
211 uncertainty (1σ) in the isoprene observations is estimated as 31%, with the sensitivity uncertainty
212 dominating.

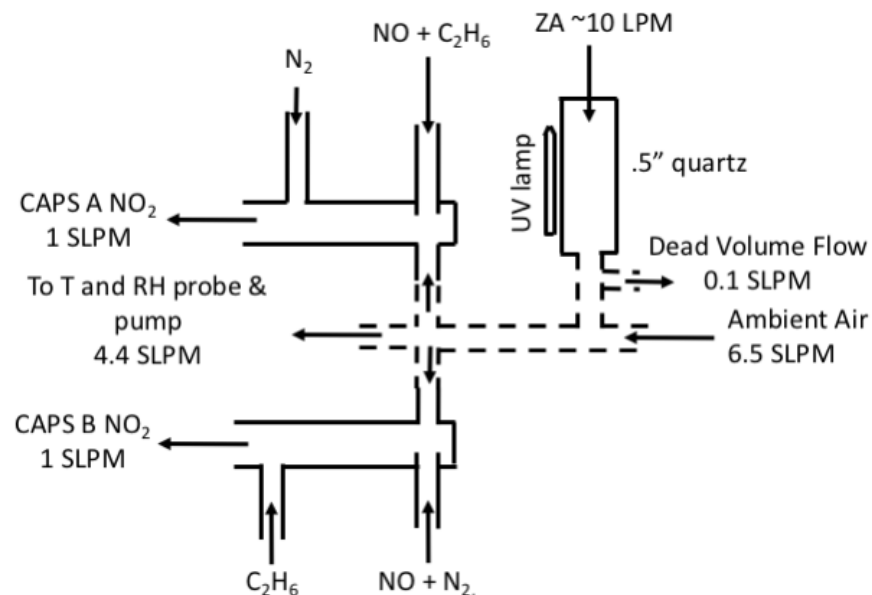
213 While there was an in-field calibration for the PTR derived isoprene, it was determined that the
214 isoprene concentration in this older calibration tank was most likely lower than the stated value, biasing
215 the PTR results. There were overlapping observations of the PTR and GC derived isoprene values from
216 the start of the campaign to 19 May, after which the GC trap was damaged. So that we have calibrated
217 isoprene observations for the duration of the campaign, we have scaled the PTR derived isoprene to GC
218 values for this overlapping period. The 1-minute averaged PTR data were averaged to the GC sampling
219 time, and a linear least squares regression was used to determine the relationship. This resulted in a fit
220 with an r^2 of 0.91 and a relationship between the two instruments as follows: $[C_5H_8]_{GC} = 0.787[C_5H_8]_{PTR} -$
221 0.15. The normalized mean bias for this relationship was 7%.

222 ***S4. Model Description***

223 To calculate the L_N/Q parameter from Sect. 3.2 of the main text, we modeled the photochemistry
224 with the Framework for 0-D Atmospheric Modeling (F0AM) version 3.1 box model (Wolfe et al., 2016).
225 The model was run with a subset of the Master Chemical Mechanism (Jenkin et al., 2003;Saunders et al.,
226 2003) version 3.3.1 (MCMv331) (Jenkin et al., 2015). F0AM was constrained with observations taken
227 during SAFS of temperature, pressure, water vapor, O_3 , NO_2 , CO, CH_4 , HCHO, methanol, acetone,
228 acetaldehyde, isoprene, propane, ethane, ethyne, monoterpenes, toluene, *n*-pentane, *n*-hexane, *n*-heptane,
229 *n*-octane, xylenes, ethyl benzene, 1,2,4-trimethylbenzene, benzene, and cyclohexane. Because there were
230 no speciated observations, all monoterpenes were assumed to be α -pinene. Likewise, observations of
231 total *m*- and *p*-xylene were assumed to be a 50% mixture. Observational constraints were averaged over
232 the 2-minute ECHAMP sampling interval, and only intervals with simultaneous observations of XO_2 , CO,
233 O_3 , NO, water vapor, isoprene, and HCHO were used. Data from the GC, which had a sampling
234 frequency lower than that of ECHAMP, were linearly interpolated to the ECHAMP sampling time. The
235 modeled intervals were further restricted to sampling at a solar zenith angle (SZA) less than 80° . Missing
236 data were linearly interpolated in time. For photolysis reactions, the model was constrained to
237 observations of J_{NO_2} . Other photolysis rates were determined from a lookup table of values calculated by

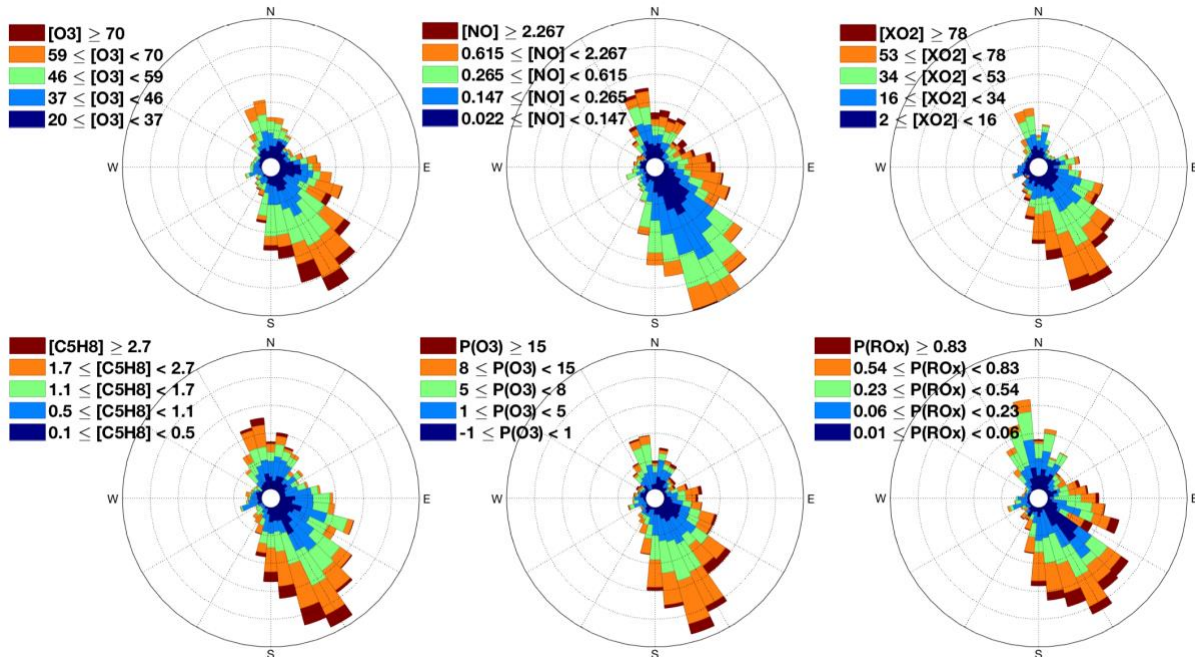
238 the TUV model as described in Wolfe et al. (2016). These values were then scaled to the observed JNO_2 .
239 The model was run forward in time with a model time-step of 1 hour, with all constrained concentrations
240 and meteorology held constant but photolysis frequencies varying with time of day. The diurnal cycle
241 was repeated for 4 days for each set of observations, which was found sufficient to bring XO_2 into steady
242 state.

243
244



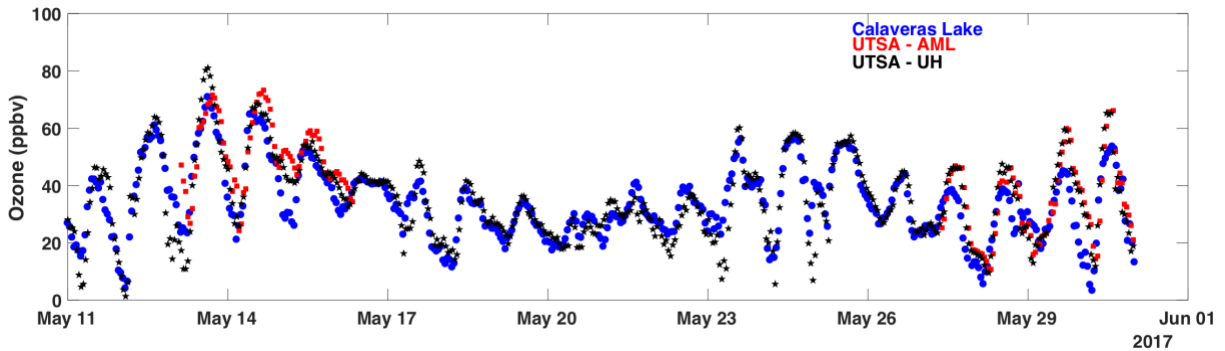
245
246 **Figure S1:** A schematic of the ECHAMP inlet used during SAFS. Dashed lines represent glass coated in
247 halocarbon wax. The ZA flow is only used during H₂O based calibrations. As drawn, the upper reaction
248 chamber (Chamber A) is in amplification mode (C₂H₆ added upstream, N₂ added downstream) and
249 reaction the lower reaction chamber (Chamber B) is in background mode. Every minute, the C₂H₆ and N₂
250 flows are switched so that the reaction chamber that was in amplification mode is then in background
251 mode and vice versa. The upstream and downstream additions are ~15.2 cm apart, and the reaction
252 chamber continues for another 66 cm before entering a filter. C₂H₆ was a 42.2% in N₂ mixture and was
253 flowed at 35 sccm; NO was a 39.2 ppmv in N₂ mixture and was flowed at 25 sccm. The N₂ flow rate was
254 35 sccm.

255
256



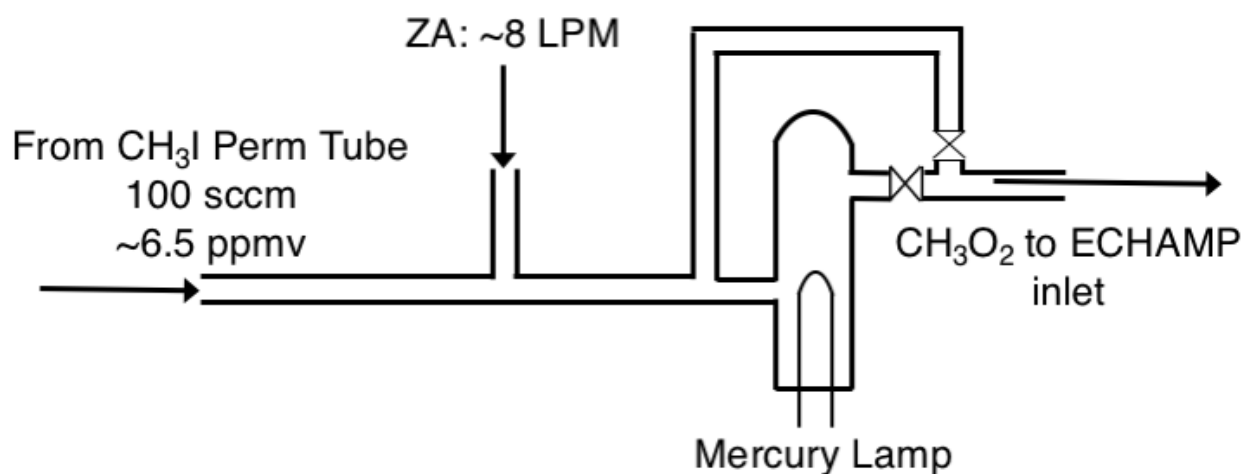
257
 258 **Figure S2:** Wind roses showing the variation in O₃ (a), NO (b), RO_x (c), isoprene (d), P(O₃), and P(HO_x)
 259 with direction for all observations at the UTSA site. Observations are separated into their 5th, 25th, 50th,
 260 75th, and 95th percentiles for each species.

261
 262
 263
 264
 265
 266
 267

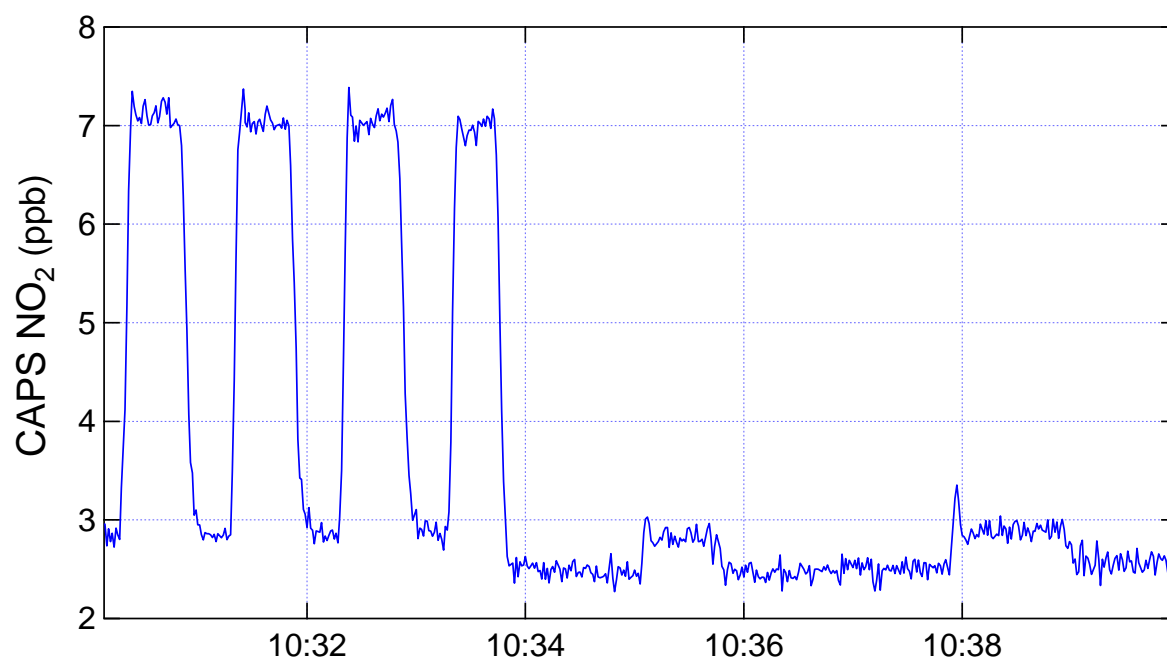


268
 269 **Figure S3:** One-hour average O₃ at the Calaveras TCEQ monitoring site (blue) and at the UTSA SAFS
 270 site, including observations from both the AML (red) and by the University of Houston (black).

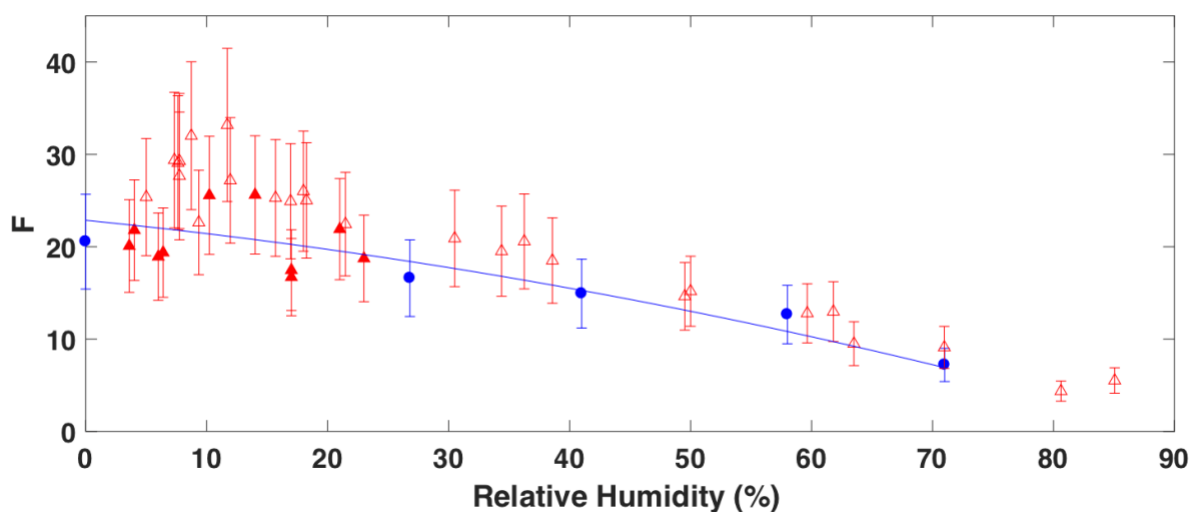
271



272
 273 **Figure S4:** A schematic of the CH₃I calibration setup. Hourglass shapes represent two-way valves. The
 274 ZA is humidified over a range of RH values from 0% to 80%.



275
 276 **Figure S5:** An example time series of CH₃I calibration data from 31 May 2017. From 10:30 to 10:34
 277 ECHAMP operated in regular amplification mode. From 10:34 to 10:40 ECHAMP was in background
 278 mode (no amplification) and the CH₃O₂ source was modulated on and off.



280
281
282 **Figure S6:** Calibration curve for ECHAMP during AQR. The results from the CH₃I (blue circles) H₂O
283 photolysis (red, filled triangles) are both shown. In addition, results from an H₂O photolysis calibration
284 conducted during a subsequent field deployment are also shown (red, open triangles). Indicated
285 uncertainties are the ECHAMP measurement uncertainty of 25% (2σ).
286

287 **Table S1:** Description of the different simulations used to calculate the variation in INO, I₂, and CH₃O₂I
288 with time in the CH₃I calibration setup. $k_{\text{CH}_3\text{O}_2+\text{I}+\text{M}}$ is the rate constant for the forward reaction of reaction
289 S12.
290

	Simulation 1	Simulation 2	Simulation 3	Simulation 4
$[\text{I}]_0 = [\text{CH}_3\text{O}_2]_0$ (pptv)	100	1000	100	1000
$k_{\text{CH}_3\text{O}_2+\text{I}+\text{M}}$ (molecules cm ⁻³ s ⁻¹)	1.0×10^{-11}	1.0×10^{-11}	1.0×10^{-10}	1.0×10^{-10}

291
292
293 **Table S2:** Rate constants at 298 K and sources for the iodine simulations. The reaction rate for Reaction
294 S12 forward was varied as described in the text and Table S1.

Reaction	k_i (cm ³ molecules ⁻¹ s ⁻¹)	Source
$\text{I} + \text{I} \rightarrow \text{I}_2$ (Reaction RS9)	3.92×10^{-13}	Jenkin et al. (1990)
$\text{I} + \text{NO} + \text{M} \rightarrow \text{INO} + \text{M}$ (Reaction RS10)	1.7×10^{-11}	Atkinson et al. (2007)
$\text{INO} + \text{INO} \rightarrow \text{I}_2 + 2\text{NO}$ (Reaction RS11)	1.3×10^{-14}	Atkinson et al. (2007)
$\text{CH}_3\text{O}_2 + \text{I} + \text{M} \rightarrow \text{CH}_3\text{O}_2\text{I} + \text{M}$ (Reaction RS12 forward)	1.0×10^{-11}	Estimate
$\text{CH}_3\text{O}_2\text{I} + \text{M} \rightarrow \text{CH}_3\text{O}_2 + \text{I} + \text{M}$ (Reaction RS12 reverse)	0	Estimate
$\text{CH}_3\text{O}_2\text{I} + \text{I} \rightarrow \text{I}_2 + \text{CH}_3\text{O}_2$ (Reaction RS13)	1.0×10^{-11}	Estimate
$\text{CH}_3\text{O}_2 + \text{NO} \rightarrow \text{NO}_2 + \text{CH}_3\text{O}$	7.7×10^{-12}	Sanders et al. (2011)

295
296
297
298
299
300
301

302 **S5. References**

303

304 Anderson, D.C, Pavelec, J., Lindsay, A., Wood, E.C.: Wall Loss Rates and the Use of Nafion
305 Tubing for Selective Measurement of Peroxy Radicals. In preparation.

306 Atkinson, R., Baulch, D. L., Cox, R. A., Crowley, J. N., Hampson, R. F., Hynes, R. G., Jenkin,
307 M. E., Rossi, M. J., Troe, J., and Subcommittee, I.: Evaluated kinetic and photochemical data for
308 atmospheric chemistry: Volume II; gas phase reactions of organic species, *Atmos. Chem. Phys.*,
309 6, 3625-4055, 10.5194/acp-6-3625-2006, 2006.

310 Atkinson, R., Baulch, D. L., Cox, R. A., Crowley, J. N., Hampson, R. F., Hynes, R. G., Jenkin,
311 M. E., Rossi, M. J., and Troe, J.: Evaluated kinetic and photochemical data for atmospheric
312 chemistry: Volume III - gas phase reactions of inorganic halogens, *Atmospheric Chemistry and*
313 *Physics*, 7, 981-1191, 10.5194/acp-7-981-2007, 2007.

314 Cantrell, C. A., Zimmer, A., and Tyndall, G. S.: Absorption cross sections for water vapor from
315 183 to 193 nm, *Geophysical Research Letters*, 24, 2195-2198, 10.1029/97gl02100, 1997.

316 Clemitshaw, K. C., Carpenter, L. J., Penkett, S. A., and Jenkin, M. E.: A calibrated peroxy
317 radical chemical amplifier for ground-based tropospheric measurements, *J. Geophys. Res.*, 102,
318 25405, 10.1029/97jd01902, 1997.

319 Creasey, D. J., Heard, D. E., and Lee, J. D.: Absorption cross-section measurements of water
320 vapour and oxygen at 185 nm. Implications for the calibration of field instruments to measure
321 OH, HO₂ and RO₂ radicals, *Geophysical Research Letters*, 27, 1651-1654,
322 10.1029/1999gl011014, 2000.

323 Jenkin, M. E., Cox, R. A., Mellouki, A., Lebras, G., and Poulet, G.: Kinetics of the Reaction of
324 Iodine Atoms with HO₂ Radicals, *Journal of Physical Chemistry*, 94, 2927-2934,
325 10.1021/j100370a036, 1990.

326 Jenkin, M. E., Saunders, S. M., Wagner, V., and Pilling, M. J.: Protocol for the development of
327 the Master Chemical Mechanism, MCM v3 (Part B): tropospheric degradation of aromatic
328 volatile organic compounds, *Atmospheric Chemistry and Physics*, 3, 181-193, 2003.

329 Jenkin, M. E., Young, J. C., and Rickard, A. R.: The MCM v3.3.1 degradation scheme for
330 isoprene, *Atmospheric Chemistry and Physics*, 15, 11433-11459, 10.5194/acp-15-11433-2015,
331 2015.

332 Lanzendorf, E. J., Hanisco, T. F., Donahue, N. M., and Wennberg, P. O.: The measurement of
333 tropospheric OH radicals by laser-induced fluorescence spectroscopy during the POPCORN field
334 campaign and Intercomparison of tropospheric OH radical measurements by multiple folded
335 long-path laser absorption and laser induced fluorescence - Comment, *Geophysical Research*
336 *Letters*, 24, 3037-3038, 10.1029/97gl02899, 1997.

337 Sanders, S. P., Friedl, R. R., Abbatt, J. P. D., Barker, J. R., Burkholder, J. B., Golden, D. M.,
338 Kolb, C. E., Kurylo, M. J., Moortgat, G. K., Wine, P. H., R.E., H., and Orkin, V. L.: *Chemical*
339 *Kinetics and Photochemical Data for Use in Atmospheric Studies*, 2011.

- 340 Saunders, S. M., Jenkin, M. E., Derwent, R. G., and Pilling, M. J.: Protocol for the development
341 of the Master Chemical Mechanism, MCM v3 (Part A): tropospheric degradation of non-
342 aromatic volatile organic compounds, *Atmospheric Chemistry and Physics*, 3, 161-180, 2003.
- 343 Schultz, M., Heitlinger, M., Mihelcic, D., and Volzthomas, A.: Calibration Source for Peroxy-
344 Radicals with Built-in Actinometry using H₂O and O₂ photolysis at 185 nm, *Journal of*
345 *Geophysical Research-Atmospheres*, 100, 18811-18816, 10.1029/95jd01642, 1995.
- 346 Wolfe, G. M., Marvin, M. R., Roberts, S. J., Travis, K. R., and Liao, J.: The Framework for 0-D
347 Atmospheric Modeling (F0AM) v3.1, *Geosci. Model Dev.*, 9, 3309-3319, 10.5194/gmd-9-3309-
348 2016, 2016.
- 349 Wood, E. C., and Charest, J. R.: Chemical Amplification - Cavity Attenuated Phase Shift
350 Spectroscopy Measurements of Atmospheric Peroxy Radicals, *Analytical Chemistry*, 86, 10266-
351 10273, 10.1021/ac502451m, 2014.
- 352 Wood, E. C., Deming, B. L., and Kundu, S.: Ethane-Based Chemical Amplification
353 Measurement Technique for Atmospheric Peroxy Radicals, *Environmental Science &*
354 *Technology Letters*, 4, 15-19, 10.1021/acs.estlett.6b00438, 2017.
355